Geochimica et Cosmochimica Acta, Vol. 69, No. 23, pp. 5585–5596, 2005
Copyright © 2005 Elsevier Ltd
Printed in the USA. All rights reserved
0016-7037/05 $30.00 + .00

doi:10.1016/j.gca.2005.07.009

Occurrence of arsenic (V) in forearc mantle serpentinites based on X-ray absorption spectroscopy study

Keiko Hattori,[1,*] Yoshio Takahashi,[2] Stephane Guillot,[3] and Bo Johanson[4]

[1]Department of Earth Science, University of Ottawa, Ottawa, K1N 6N5, Canada
[2]Department of Earth and Planetary Systems Science, Hiroshima University, Hiroshima, 739-8526, Japan
[3]Laboratoire de Dynamique de la Lithosphere, CNRS, UCB-Lyon, 69622, Villeurbanne, France
[4]Geological Survey of Finland, Espoo, FIN-02151, Finland

(*Received August* 10, 2004; *accepted in revised form July* 20, 2005)

Abstract—We examined As concentration, mineralogical site, and oxidation state in the serpentinites associated with the Tso Morari eclogitic rocks in the Indus suture zone, northwest Himalaya, to examine how highly fluid-soluble elements like As are transferred from slabs to arc magmas in subduction zones. The serpentinite samples represent hydrated peridotites at the base of the mantle wedge beneath Eurasia, and were exhumed from a depth of ~100 km during subduction of the Indian continental margin. The bulk serpentinite samples contain total As concentrations ranging from 6 to 275 ppm. Arsenic in the samples is most likely present with magnetite and antigorite, since electron probe analysis yielded up to 90 ppm As in these minerals. X-ray absorption near-edge structure spectra indicate that As in serpentinites is mostly As(V) and that the neighboring atoms of As are O, although there are minute grains of sulfides and arsenides. The ratio of As(V) to total As is greater in samples with higher As contents, suggesting that the major source of As was oxidized As(V), introduced to the mantle wedge. Arsenic(V), originally adsorbed on Fe-oxides in slabs and overlying sediments, was most likely liberated during their subduction and incorporated subsequently in the overlying mantle wedge. Our data constrain the introduction of As into the mantle wedge at relatively shallow levels, much shallower than 25 km. Arsenic incorporated in the serpentinites was transported to deeper levels by mantle flow downward along the subduction zone, to be subsequently exhumed together with eclogitic rocks. *Copyright © 2005 Elsevier Ltd*

1. INTRODUCTION

Arc magmas are enriched in soluble elements, such as alkalis and alkali-earth elements, compared to midoceanic ridge basalts (MORB). This enrichment is attributed to their transport in fluids from subducting slabs and sediments to partial melts in overlying mantle wedges (e.g., Gill, 1981). Among these soluble elements, several chalcophile elements are highly enriched in arc magmas, especially at volcanic fronts, including As (Ryan et al., 1995; Leeman, 1996; Noll et al., 1996). Arsenic is soluble in aqueous fluid even at low temperatures, as demonstrated by high concentrations of As in surface and ground waters (e.g., Smedley and Kinniburgh, 2002). This raises the question of how such a mobile element can be transferred from sediments and slabs to a partial melt in the hot interior of mantle wedges.

We examined serpeninites in the Tertiary subduction complex of the Ladakh area, northwest Himalayas. The serpentinites are associated with the Tso Morari eclogitic unit, 100 × 50 km in size (Fig. 1), which was once the margin of the Indian continent before being subducted beneath Eurasia after collision of the two continents (Guillot et al., 2000, 2001). The eclogites reached a depth of ~100 km and a temperature of ~600°C at ~50 Ma before being exhumed together with the serpentinites (Guillot et al., 2000, 2001). Thus, the serpentinites represent hydrated peridotites at the base of mantle wedge in the paleosubduction zone. Bulk chemical compositions of insoluble elements and chromite compositions confirm that the serpentinites were originally refractory mantle peridotites, and that they are enriched in soluble elements, including As and Sb, during their hydration in the mantle (Fig. 2; Hattori and Guillot, 2003).

Arsenic has an oxidation state that ranges from −3 to +5. It is an important minor and trace component of rock-forming minerals in Earth's crust, and commonly replaces S(VI) and P(V). We determined the As contents of various minerals in our serpentinite samples using an electron microprobe under conditions of high accelerating voltage and specimen current, to obtain a low detection limit. We also conducted X-ray absorption fine structure (XAFS) spectroscopy, consisting of X-ray absorption near-edge structure (XANES) and extended X-ray absorption fine structure (EXAFS) spectroscopy, to identify the oxidation state of the As, and the atoms around As. We discuss the occurrence of As in the samples, and transfer mechanism of As from the slab to the mantle wedge, and eventually to arc magmas.

2. SAMPLES AND ANALYTICAL PROCEDURES

2.1. Samples

Samples were collected from discontinuous lenses of serpentinites, 100 × 1000 m in size, along the Zildat fault in contact with the Tso Morari eclogitic unit (Fig. 1). All serpentinite samples have similar bulk chemical compositions, with high concentrations of compatible elements; high Cr (~2000 ppm), Ni (>2000 ppm), and MgO (>40 wt%), and low Al_2O_3 (<1.0 wt%) (Table 1). Overall high contents of platinum group elements and low Re in bulk samples and high Cr/(Cr + Al), ~0.8, in chromite are consistent with the refractory mantle origin of the samples (Guillot et al., 2000, 2001). Their refractory mantle origin is further supported by a gradual change in concentra-

* Author to whom correspondence should be addressed (khattori@uottawa.ca).

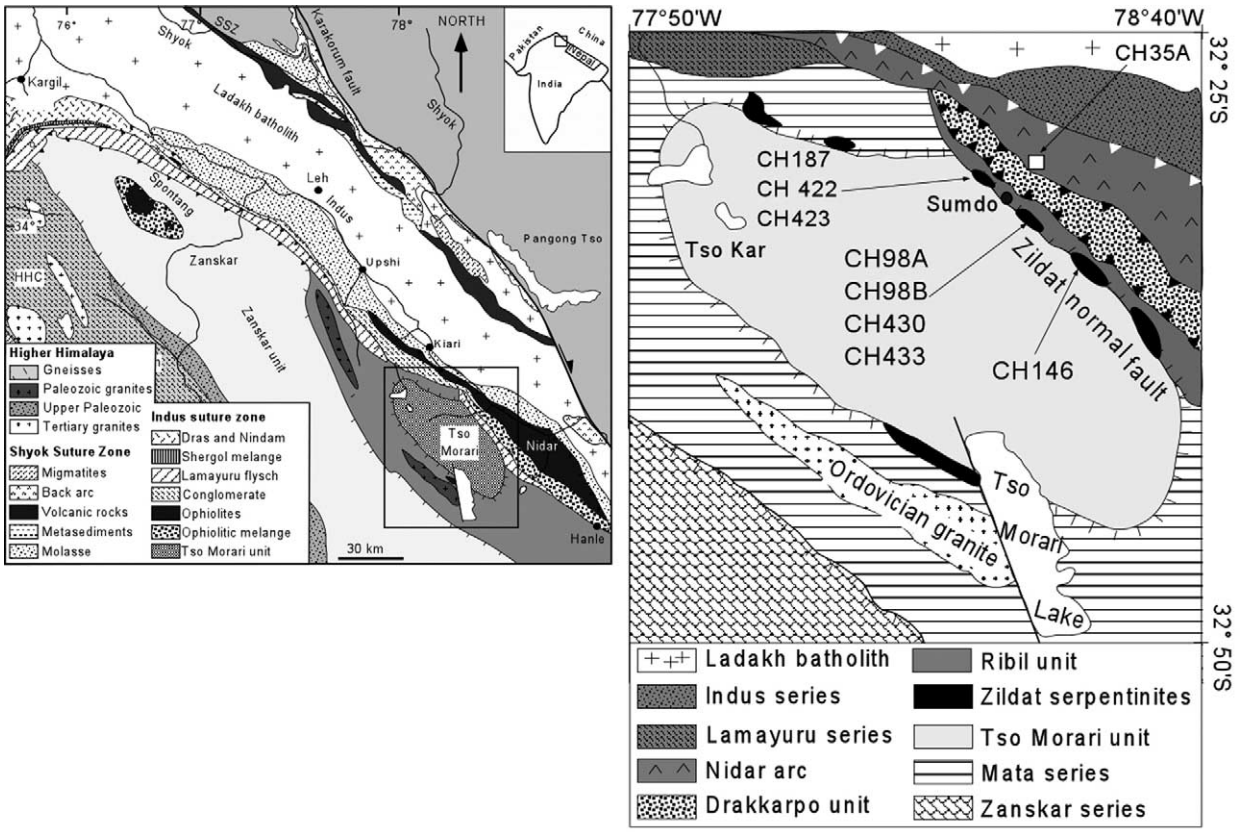

Fig. 1. Geological map of Lakakh area in northwestern India, showing sample locations in Indus suture zone. Map modified after Guillot et al. (2001).

tions, from highly compatible Mg to moderately compatible Zr (Fig. 2). However, the serpentinites are enriched in soluble elements, such as As, Sb, Pb, light rare earth elements (REE), and Sr (Fig. 2; Hattori and Guillot, 2003).

The serpentinite samples consist mainly of antigorite and minor chrysotile, chlorite, talc and chromite. Secondary magnetite occurs on the rims, ~50 μm wide, of chromite and as fine ($<$ 10 μm) dusty dissemination in antigorite. Coarse-grained, $>$ 20 μm, magnetite is present, but rare and these grains are used to obtain the As concentrations. Chrysotile and chlorite crystallized later, forming veinlets. Sulfide minerals are largely absent, except for minute ($<$ 5 μm) grains of millerite (NiS) and heazlewoodite (Ni_3S_2) in several samples.

For comparison, we selected one serpentinite sample, CH 35A, east of the Zildat fault (Fig. 1b). This is a representative sample at the base of the Nidar complex, which formed as an oceanic arc developed in the Tethyan Sea, and later was obducted over the Indian margin during early Paleocene (Mahéo et al., 2004). The sample shows a bulk composition comparable to the serpentinite samples from the forearc mantle wedge, but the chromite grains have lower Cr#, ~0.6 (Guillot et al., 2001), than that for the latter. The composition and the geological setting suggest that the sample is most likely an uppermost oceanic mantle peridotite.

2.2. X-ray Absorption Spectroscopy

The XAFS spectroscopic tool evaluates the local atomic structure around a specific element in a variety of media, even when the element occurs at a low concentration. XAFS spectroscopy has been applied to problems in earth science over 25 yr, yet is new to petrological studies, and thus the principles of the technique are described briefly. The spectroscopic method relies on excitation of electrons to a higher energy level or delocalized state by bombarding the material with X-rays. This excitation of electrons is recorded as absorption of incident X-rays or fluorescence of the excited atoms. When the energy of incident X-rays is low, there is essentially no absorbance of X-rays because no excitation of electrons. When the energy is sufficiently high, a large increase in absorbance occurs, thus producing an absorption edge on the plot of absorbance vs. increasing incident X-ray energy. The position of the edge and its intensity are related to the binding energies of the valence orbitals. The absorption spectrum near the edge, XANES, thus provides information on the oxidation state of the absorbing atom. On the higher energy side of the edge, the absorbance gradually decreases with increasing energy, but it shows a series of oscillations due to interference of photoelectrons emitted from the central atom by the neighboring atoms. The oscillation pattern depends on the number of neighboring atoms (coordination number), the type of neighboring elements, and the distance between the absorber and the atoms involved in backscattering (interatomic distance). EXAFS spectroscopy utilizes this oscillatory behavior of the absorption above a major absorption edge. This new field of study has recently been reviewed in a book edited by Fenter et al. (2002). Other informative papers include Brown et al. (1988) and O'Day et al. (2004).

The X-ray absorption spectroscopy analysis was conducted on powdered bulk samples at BL-12C of the Photon Factory (KEK, Tsukuba, Japan) and at BL01B1 of SPring-8 (Hyogo, Japan). The incident beam was regulated with a Si (111) double-crystal monochromator and focused on samples using a bent cylindrical mirror to a size of 1 $\times$ 0.5 mm^2. Spectra were collected under ambient conditions ($\sim$ 20°C and 1 bar) in the fluorescence mode by scanning the energy at 0.25 eV steps in X-ray absorption near-edge structure region and recorded using a 19-element Ge semiconductor detector. Most samples were scanned twice and samples with significant noise in the spectra were subjected to a third scanning. During the scans, the spectra and sample temperature did not show any significant changes. The peak position of reference materials, $As_2^{III}O_3$ and $As_2^{V}O_5$, did not shift more than 0.25 eV throughout this study and the duplicate runs of samples suggest that

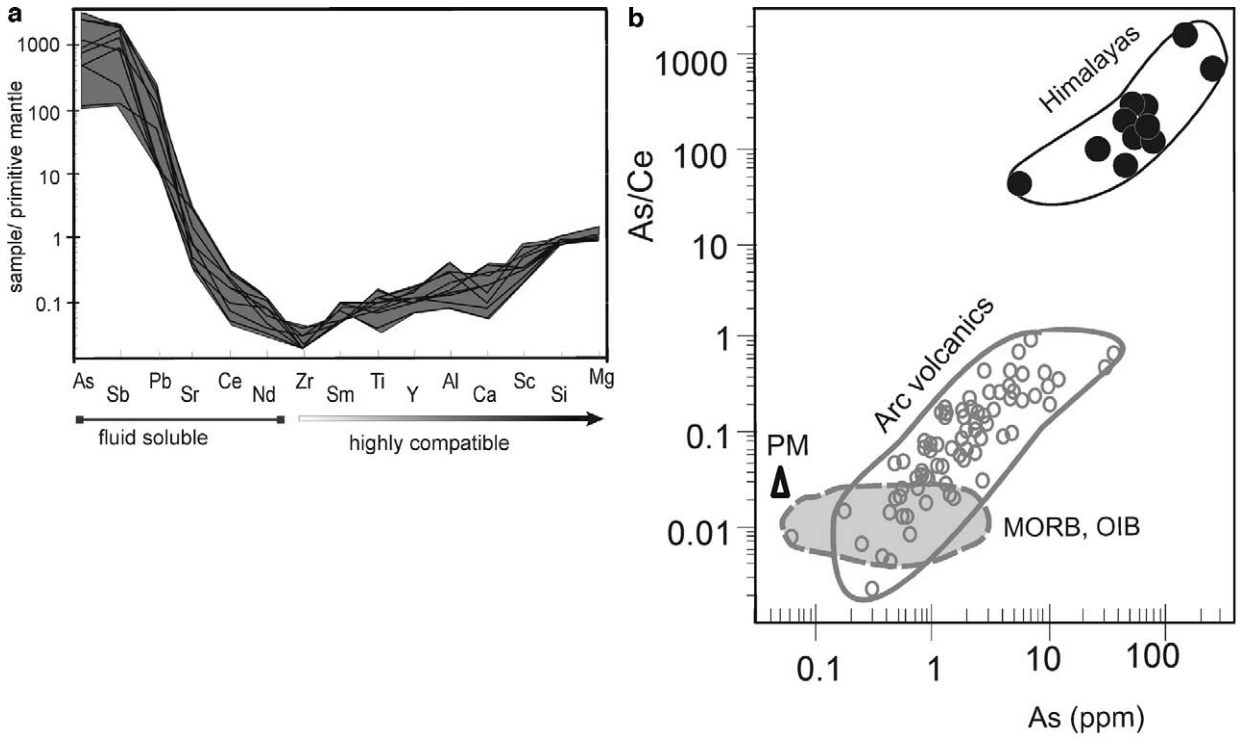

Fig. 2. (a) Composition of serpentinites normalized to primitive mantle. Arsenic and Sb are similar in compatibility to LREEs (Noll et al., 1996), but they are placed on the left to highlight their fluid-soluble enrichment. Elements from Zr to the right are placed in order of their increasing compatibility with mantle minerals. Primitive mantle values are from McDonough and Sun (1995). Modified after Hattori and Guillot (2003). (b) Arsenic and As/Ce ratios of serpentinites compared to those of primitive mantle (PM; McDonough and Sun, 1995), midoceanic ridge basalts (MORB), and oceanic island basalts (OIB; Noll et al., 1996). Arc magmas include data from Pinatubo, Philippines (Bernard et al., 1996), Esan (Noll et al., 1996), basalt rock standards JB-2 and JB-3 from Geological Survey of Japan (Ando et al., 1989), volcanic rocks in Japan (Togashi et al., 2000), volcanic rocks in Hishikari area in southern Kyushu and Miyake-jima volcano, Japan, and Medvhizya and Brat volcanoes in Kuril arc, Russia (Volynets, 1994; Noll et al., 1996).

the uncertainties of the data are less than 10%. Energy was calibrated by defining the main absorbance peak of $As_2^{III}O_3$ at 11.866 keV. The detailed analytical procedure is described by Takahashi et al. (2003, 2004).

The proportion of As(V) relative to total As was calculated from XANES spectra of samples and two reference materials; $As_2^{III}O_3$ and $As_2^{V}O_5$. The calculation involves normalization of spectra and fitting the linear combination of the end members in the energy region between 11.852 and 11.887 keV, as reported in Takahashi et al. (2003). The least-square fitting was processed using Solver, an add-in program of Microsoft Excel.

EXAFS spectra were recorded around the As K-edge over a range of 11.5 to 12.8 keV for sample CH 187 and reference materials of $NaAsO_2$, As_2O_3, and natural enargite (Cu_3AsS_3). EXAFS data were analyzed using the Rigaku REX 2000 program (version 2.3) and FEFF7 (Zabinsky et al., 1995; Ankudinov and Rehr, 1997) after the initial structural data were obtained with the ATOMS program (Ravel, 2001). Background was removed using five cubic spline curves following subtraction of preedge and postedge background and normalization to the edge values. The k^3-weighted EXAFS function, $\chi(k)k^3$, was Fourier transformed from k space ($Å^{-1}$) into R space (Å) over the k-range 2.7 to 10.2 $Å^{-1}$, which yielded a radial structure function (RSF). Inverse Fourier transformation of a portion of the RSF was performed for the first shell of each sample. The experimental spectra of EXAFS were least-square fitted to theoretical EXAFS functions generated using the computer code FEFF7 (Zabinsky et al., 1995). This yielded the average distance between As and the neighboring atoms, coordination number of As, and Debye-Waller factor for the first As atomic shell.

2.3. Total Sulfur Concentrations and Isotope Analysis

Total sulfur was extracted as H_2S from ~35 g of bulk rock powder by placing the samples together with KIBA reagent (Sasaki et al., 1979) in a Pyrex glass flask. The H_2S was precipitated as Ag_2S in $AgNO_3$ solution and the weight of Ag_2S was used to calculate the concentration of total S in the samples. To reduce the blank contribution of S from the apparatus, the Pyrex flask was washed with dilute HF before each sample preparation. This cleaning reduced the blank contribution to less than 0.10 mg of Ag_2S (0.014 mg S). The Ag_2S was mixed with V_2O_5 (1:2 weight ratio) in Al foil and placed in an elemental analyzer (Carlo Erba 1110) to yield SO_2 at 1700°C for isotopic ratio measurements.

2.4. Atomic Absorption Spectroscopy

The concentration of As in bulk rock was determined in 0.5-g aliquots of samples digested by aqua regia at 95°C for 2 h, then diluted to 10 mL with H_2O. The solution was mixed with KI-$C_6H_8O_6$ solution, followed by analysis using a Perkin-Elmer 2100 atomic absorption spectrometer with FIAS-400 hydride generating system. The detection limit is 0.1 ppm and the overall uncertainty based on duplicate analysis is ± 10% of the quoted value. The analytical procedure is essentially the same as that described by Hageman et al. (2002).

2.5. Electron Microprobe

Arsenic contents of various mineral phases were determined using a Cameca SX 50 electron probe equipped with four wave-length energy dispersive spectrometers. Analytical conditions were 35 kV and beam

Table 1. Composition of serpentinite samples.

	Method	CH 422	CH 423	CH 433	CH 98A	CH 98B	CH 146	CH 187	CH 35A
As (ppm)	[a]	27.3	49.2	62.1	275	54.1	6.0	145	56.6
As(VI)(% of total)	[b]	53	73	83	59	75	43	83	4
S (ppm)	[c]	8	51	<4	34	<4	6.6	41	<4
$\delta^{34}S$ (‰)	[d]	n.d.	−6.5	n.d	+4.3	n.d	n.d	−0.5	n.d
SiO_2(%)	[e]	39.6	37.4	39.2	35.1	40.2	40.6	39.4	38.7
TiO_2(%)	[e]	0.02	0.008	0.013	0.03	0.015	0.024	0.023	0.02
Al_2O_3(%)	[e]	1.6	0.31	0.56	0.54	0.37	0.77	1.09	0.49
Fe_2O_3(% total Fe)	[e]	7.99	6.60	7.39	6.83	7.54	7.59	8.99	7.58
MnO (%)	[e]	0.089	0.125	0.104	0.127	0.10	0.093	0.105	0.1
MgO(%)	[e]	37.0	41.9	37.5	40.0	41.8	36.7	38.0	38.6
CaO(%)	[e]	0.482	0.201	1.403	0.64	0.29	1.05	0.33	0.65
P_2O_5(%)	[e]	0.005	0.024	0.006	0.005	0.006	0	0.001	0.003
LOI(%)	[f]	13.1	13.2	13.5	16.7	9.7	13.1	11.8	13.8
SUM		99.88	99.72	99.65	99.89	99.99	99.88	99.73	99.88
V (ppm)	[e]	45	11	34	19	18	34	37	28
Cr (ppm)	[e]	2290	2770	2370	2720	2600	2580	2780	2120
Co (ppm)	[e]	100	114	97	97	110	93	113	107
Cu (ppm)	[g]	8.74	6.68	8.57	5.05	6.34	13.22	5.21	4.64
Ni (ppm)	[e]	2060	2760	1980	2260	2830	2260	2390	2220
Zn (ppm)	[e]	34	27	44	51	54	30	32	49
Nb (ppm)	[h]	0.98	0.37	0.14	0.82	0.56	0.07	0.08	0.84
Sb (ppm)	[a]	1.32	7.25	4.68	11.97	10.07	0.69	10.2	5.08
Pb (ppm)	[h]	2.15	2.44	1.95	13.7	2.64	7.83	33.7	19.3
Sc (ppm)	[h]	11.3	3.2	5.5	5.3	3.8	5.7	7.9	5.3
Rb (ppm)	[i]	0.108	0.11	0.14	0.075	0.067	0.033	0.11	n.d.
Sr (ppm)	[i]	9.1	6.6	55	22.8	13.1	30.4	6.9	n.d.
Nd (ppm)	[i]	0.131	0.063	0.152	0.058	0.076	0.049	0.041	n.d.
Sm (ppm)	[i]	0.04	0.0186	0.041	0.02	0.0213	0.0194	0.0185	n.d.

[a] Hydride generator with atomic absorption spectrometer after aqua regia digestion.
[b] XANES fit with ±10% uncertainty.
[c] Ag_2S precipitation of H_2S released from samples in Kiba reagent (Sasaki et al., 1979).
[d] Gas-source mass spectrometer after combustion of Ag_2S with V_2O_5.
[e] X-ray fluorescent spectrometer.
[f] Weight loss after heating samples for 1.5 h at 1100 C.
[g] ICP-MS after *aqua regia* digestion.
[h] ICP-MS after digestion with HF-$HClO_4$-HNO_3-HCl.
[i] Isotopic dilution analysis using spike solutions containing enriched ^{85}Rb, ^{84}Sr, ^{142}Nd, and ^{147}Sm.
n.d. = not determined.

current of 500 nA for most minerals. The As-K_α peak was measured using a LiF crystal for 600 s, and backgrounds were each measured for 300 s. High electron current, voltage and long counting time lowered the detection limit of As to 14 to 16 ppm in all phases. The detection limit was defined as $3 \times \sqrt{B} \times \sqrt{t}$, where B is the background counts and t the counting time. The beam size was ~0.25 to 0.5 μm in diameter. For antigorite, the beam size was widened to 25 to 30 μm and the current was lowered to 100 nA to prevent rapid disintegration of the mineral during analysis. The standard for As was natural cobaltite containing 45.2 wt% As, obtained from Astimex Ltd. The analytical procedure is essentially the same as that described by Hattori et al. (2004).

3. RESULTS

The serpentinite bulk-rock samples contain high concentrations of As, ranging from 6 to 275 ppm (Fig. 2; Table 1). Sulfur concentrations were all very low, less than 51 ppm S, and three samples yielded S concentrations below the detection limit of 4 ppm S. The S isotopic compositions show a relatively narrow spread, ranging from −6.5 to +4.3‰ (Table 1).

Electron microprobe study identified minute (< 2 μm) Ni-sulfide minerals with high As, up to 0.25 wt% in heazlewoodite (Table 2). After extensive search for metallic minerals, we found one tiny, < 2 μm, grain of arsenide. The composition is close to orcelite ($Ni_{5-x}As_2$) and maucherite ($Ni_{11}As_8$) (Table 3) and it is likely that this minute grain is a mixture of two or more phases. Nickel arsenides are rare in nature, and all known occurrences are related to hydrothermal veins. Detailed examination of samples did not identify any other As minerals. The concentration of As in other phases is much lower. Chromite shows As concentrations below the detection limit of 16 ppm. Most magnetite rimming chromite and small grains of magnetite in antigorite contain low As, below the detection limit of 16 ppm, but several grains contain As up to 66 ppm (Table 2). It was difficult to obtain the precise concentrations of As in antigorite because the mineral was not stable under high electron current and voltage, requiring the electron beam to be widened to 25 to 30 μm. Many antigorite grains are smaller than the beam size and most grains contain numerous dusty inclusions of magnetite. Clear areas of large antigorite grains yielded varying As values, with one analysis close to 90 ppm As.

The XANES of As shows strong absorption features at around 11.870 keV, which is similar to the peak for As(V)-bearing species in which As is bonded to oxygen such as in $As_2^{V}O_5$ and adamite, $Zn_2(As^{V}O_4)(OH)$ (Figs. 3 and 4). The observed XANES pattern is similar to those of As^{V}-O phases

Table 2. Arsenic concentration of various minerals.

Mineral	As (ppm)	Remarks
	Sample CH 98 A	
Heazlewoodite	769	Grain is enclosed in an aggregate of antigorite
Heazlewoodite	751	Ditto
Pentlandite	2300	Ditto
Pentlandite	1900	Ditto
Chromite	<16	Core of chromite rimmed by magnetite
Magnetite	48	Rim of chromite grain
Magnetite	25	Rim of chromite grain
Magnetite	45	Small grain in an aggregate of antigorite
Magnetite	35	Small grain in an aggregate of antigorite
	Sample CH 187	
Pentlandite	564	Grain is enclosed by an aggregate of antigorite
Pentlandite	684	Grain is enclosed by an aggregate of antigorite
Pentlandite	697	Grain is enclosed by an aggregate of antigorite
Chromite	<16	Core of chromite rimmed by magnetite
Magnetite	48	Magnetite rimming chromite
Magnetite	25	Magnetite rimming chromite
Magnetite	45	Small grain of magnetite enclosed in an aggregate of antigorite
Magnetite	35	Small grain of magnetite enclosed in an aggregate of antigorite
Antigorite	66	Coarse-grained antigorite
Antigorite	89	Rim of coarse-grained antigorite
Antigorite	69	Core of coarse-grained antigorite

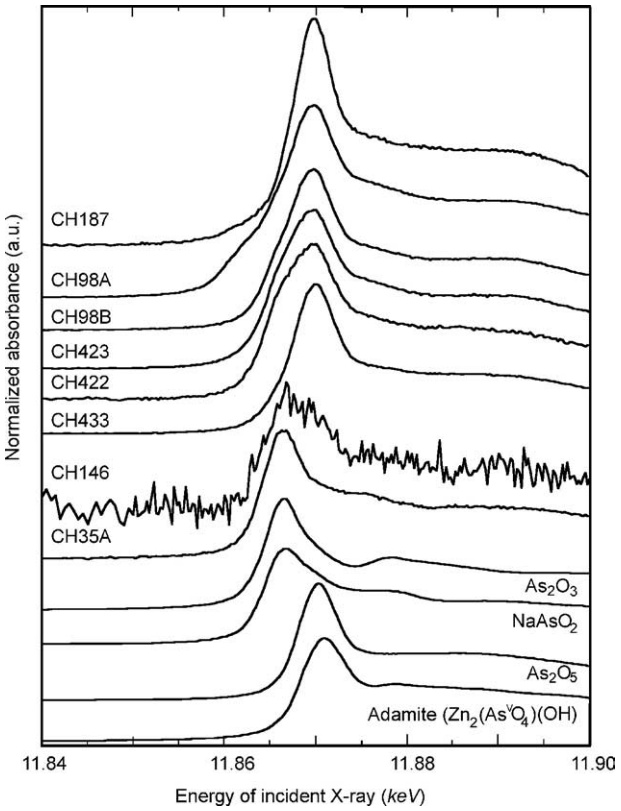

Fig. 3. Arsenic K-edge XANES spectra of serpentinite samples and reference materials of pure oxides; $As_2^{III}O_3$, $As_2^{V}O_5$, $NaAs^{III}O_2$ and adamite, $Zn_2As^{V}O_4(OH)$. a.u. = arbitrary units.

reported by Hugging et al. (1993) and Takahashi et al. (2003). The peak position of Sample CH 35A, collected at the base of the Nidar ophiolite, shows the maximum absorption at a significantly lower energy, ~11.866 keV, than the other samples, and this position is similar to that of $As_2^{III}O_3$ and $NaAs^{III}O_2$ (Fig. 3).

Using the normalized spectra of the samples and reference materials of As_2O_3 and As_2O_5, the fractions of As(V) relative to total As was calculated from XANES spectra (Figs. 4a,b). The fractions vary from 4 to 84%. Sample CH 35A, from the base of the Nidar ophiolite, shows the lowest calculated fraction of As(V), 4%, but this is negligible given the uncertainty of ± 10%. Bulk-rock samples that contain greater than ~60 ppm As show uniformly high fractions of As(V), >60% (Fig. 5), and there is a positive correlation between the As contents and As(V) fractions in samples with lower As concentrations. Thus, higher proportions of As(V) are found in samples with higher concentrations of total As, excluding the sample from the Nidar ophiolite (Fig. 5), which does not plot on the correlation. The data are consistent with this sample having an origin different from the rest of samples.

Table 3. Composition of arsenide in CH 187.[a]

	wt%	Atomic %
Fe	0.11	0.14
Ni	49.7	58.5
As	43.0	39.6
Sb	2.68	1.52
S	0.08	0.16
Te	0.09	0.05

[a] Concentrations of Mn, Co, and Zn are <0.01 wt%.

The XANES spectra suggest that O is mostly the neighboring atoms of As in the samples. This is supported by RSF computed from the EXAFS spectra (Fig. 6). The peak maximum of RSF for the sample occurs at lower R than those for $NaAs^{III}O_2$, $As_2^{III}O_3$ and enargite (Cu_3AsS_4) (Fig. 6). These results confirm that As in the sample is predominantly As(V) and that the neighboring atoms are mostly O.

The bond distance between As and O, and the coordination number of As, are quantitatively derived for samples and reference materials using the EXAFS fits (Table 4). For reference materials, we obtained coordination numbers of 3.2 and distances of 1.79 Å between As and O for both $As_2^{III}O_3$ and $NaAs^{III}O_2$ (Table 4). The values are in good agreement with respective values of 3 and 1.79 Å for $As_2^{III}O_3$ and 3 and 1.68 to 1.83 Å for $NaAs^{III}O_2$, based on crystallographic studies by Pertlik (1978) and Emmerling and Roehr (2003), respectively. Our estimate of 2.19 Å as the distance between As and S in enargite (Cu_3AsS_4) is similar to the distance of 2.21 to 2.22 Å based on a crystallographic study (Henao et al., 1994). These excellent agreements with crystallographic results of the reference materi-

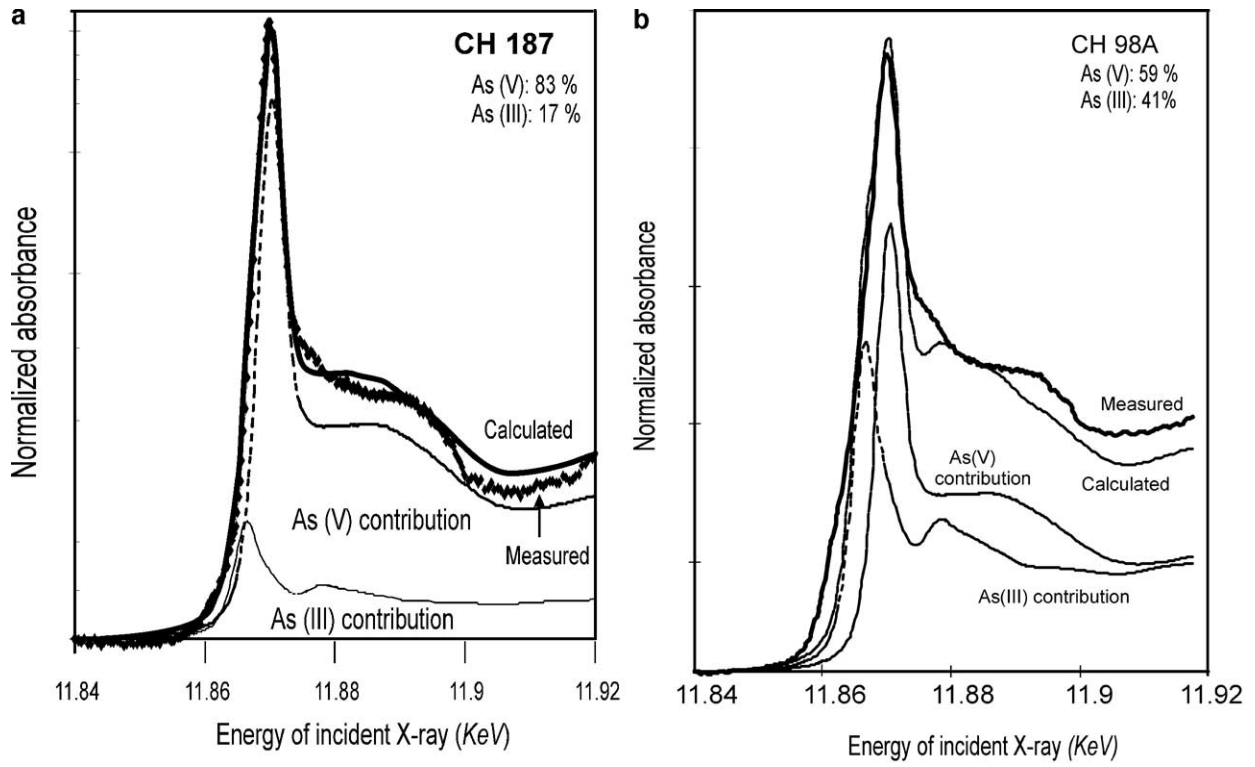

Fig. 4. Arsenic K-edge XANES spectra of samples CH 187 and CH 98A, and calculated spectra fitting based on two reference materials, As_2O_3 and As_2O_5. Calculation conducted after normalization of XANES spectra for samples and reference materials.

als validate the use of EXAFS-based calculations for our samples.

Sample CH187 yielded an average bond distance between As and neighboring atoms of 1.68 Å (Table 4). This is similar to the average As^{V}-O distance, 1.68 to 1.69 Å, in arsenate $(As^{V}O_4)^{2-}$ that is not combined with H (e.g., Mihajlović and Effenberger, 2004; Locock et al., 2005). The result confirms that As is bonded to O and that most of the As is indeed As(V)

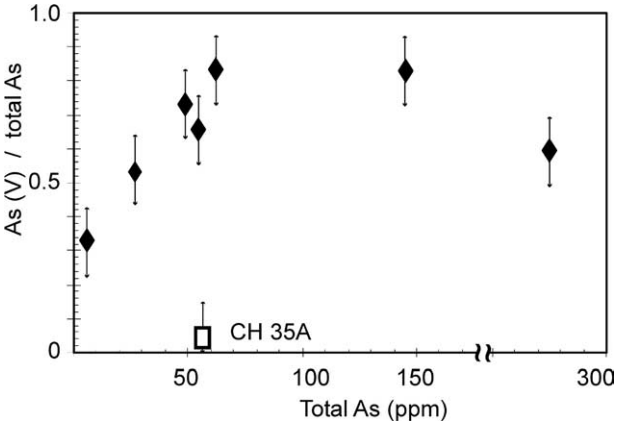

Fig. 5. Concentrations of total As vs. proportion of As (V) to total As in Tso Morari serpentinite samples. Proportion of As(V) calculated using absorption peak of reference As oxides, $As_2^{V}O_5$ and $As_2^{III}O_3$. Error bars show uncertainty of ±10%.

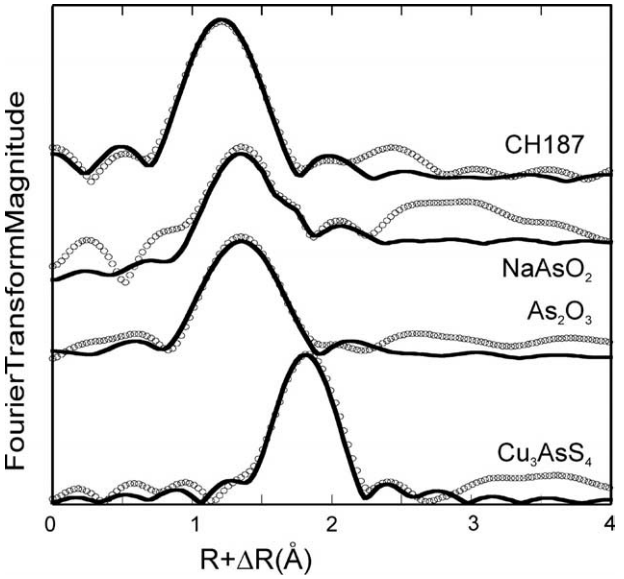

Fig. 6. Radial structure function (RSF) spectra of As, derived from EXAFS spectroscopy data. Spectrum of sample CH 187 compared to those of $NaAs^{III}O_2$, $As_2^{III}O_3$, and natural enargite (Cu_3AsS_3). Circles = original EXAFS spectra; solid lines = fitted spectra. Fourier transforms are not corrected for phase shifts; distances between As and neighboring atoms shown in RSF diagram are shorter than true distance. Quantitative estimates of distance between As and neighboring atoms, and coordination number of As are listed in Table 4.

Table 4. Arsenic EXAFS spectra parameters of the first neighboring atom.

	Calculated based on EXAFS spectra[a]						Crystallographic data[b]	
Sample	A-B	CN	R (Å)	σ^2 (Å^2)	ΔE (eV)	Residual (%)[c]	CN	R (Å)
				Reference materials				
As_2III AO_3	As-O	3.3	1.79	0.004	6.2	0.4	3	1.79
NaAsIII AO_2	As-O	3.2	1.78	0.008	7.6	1.8	3	1.83, 1.82, 1.68
Enargite Cu_3AsS_4	As-S	4.3	2.19	0.004	9.5	0.3	4	2.21, 2.22
				Sample				
CH 187	As-O	5.2	1.68	0.004	3.5	0.1		

[a] A-B = absorber-back scatterer atom pair in the material; CN = coordination number (±20%; O'Day et al., 1994); R = interatomic distance (±0.02 Å; O'Day et al., 1994); σ^2 = Debye-Waller mean-square disorder parameter; ΔE = energy shift between the value determined through experimental and the final fitted value after computation.

[b] References for crystallographic data of As_2O_3, $NaAsO_2$, and enargite (Cu_3AsS_4) are Pertlik (1978), Emmerling and Roehr (2003), and Henao et al. (1994), respectively.

[c] Residual to total proportion in R space.

in the sample, since the ionic radius of As(V) is smaller than that of As(III).

4. DISCUSSION

4.1. Possible Sites of Arsenic in Serpentinites

4.1.1. Sulfide minerals

Arsenic is a chalcophile element with strong affinity for S, and sulfide minerals are considered to be the major hosts of As in a variety of crustal rocks (e.g., Onishi and Sandell, 1955). Sulfide grains in our samples are locally high in As, up to 2500 ppm (Table 2), but the limited and minute grains of sulfide phases likely host only a small fraction of the total As. First, the abundance of sulfide minerals is very low. The concentrations of total S vary from below the detection limit of 4 ppm to a maximum of 51 ppm (Table 1). Using the concentration of S in bulk rocks and sulfide mineralogy, the maximum amount of As in our whole rocks that can be fixed in sulfides is estimated to be less than 0.4 ppm As, even if sulfides contain 2000 ppm As. Thus, the As contained by sulfides in each sample is less than ~0.8% of the total As in the samples.

Secondly, XANES spectra of our samples do not show evidence for a contribution of As from sulfide minerals. Arsenic in sulfide minerals occupies the cation site, such as realgar (AsS) and orpiment (As_2S_3), or forms dianions with S, such as $(AsS)^{2-}$ in arsenopyrite (FeAsS) and pyrite (Zachariáš et al., 2004). In either case, As in sulfides shows distinctly different X-ray absorption spectra from As in oxides, with the peak absorption at much lower energy sites than those of As oxides (Savage et al., 2000; Takahashi et al., 2003). Thirdly, As in our samples shows a short, ~1.7 Å, average bond length between As and adjacent elements compared to the bond length of As-S in sulfide minerals (Fig. 6, Table 4). Other minerals also have short As-S distance. For example, the As-S distance of realgar is 2.23 Å (Pertlik, 1994) and that of arsenopyrite 2.35 Å (Morimoto and Clark, 1961). The bond length of our samples is even shorter than that of As^{III}-O in $NaAs^{III}O_2$ and $As_2^{III}O_3$ (Fig. 6, Table 4). This indicates the predominant occurrence of As in the samples is As^{V}-O because As(V) is much smaller than less charged As (III).

4.1.2. Other minerals

Arsenic forms arsenate ($As^{V}O_4$) with a variety of metals, such as scorodite ($Fe^{III}As^{V}O_4$), pharmacosiderite [$KFe_4^{III}(As^{V}O_4)_3(OH)_4\ 6H_2O$], erythrite [$Co_3(As^{V}O_4)_2 \cdot 8H_2O$)], and annabergite [$Ni_3(As^{V}O_4)_2 \cdot 8H_2O$]. However, these minerals are very unlikely to be present in our samples. The formation of scorodite requires high Fe contents and highly oxidized conditions compared to the magnetite-hematite fO_2 buffer (Figs. 7a,b). Hematite has not been found in the serpentinites. Erythrite and annabergite, hydrated Co and Ni arsenate minerals, are highly soluble and only are found at the surface overlying weathered Ni-Co sulfide deposits, where abundant metals and As(V) are available. Such conditions are highly unlikely in mantle serpentinites.

Arsenate($As^{V}O_4$) may substitute for $P^{V}O_4$ in apatite [$Ca_3(PO_4)_2$] and pharmacolite ($CaHPO_4$). It is not easy to detect trace amounts of phosphate minerals in samples because of their inconspicuous optical and physical properties. We consider that they are unlikely hosts of As in our samples, although we can not rule out this possibility. Our samples contain low concentrations of CaO (< 1.4 wt %) and P_2O_5 (< 0.024 wt %). Secondly, there are no positive correlations between As and P and between As and Ca contents (Table 1). Thirdly, apatite has not been reported in depleted-mantle peridotites. Furthermore, P is not considered to be a mobile element, incorporated from slabs into overlying mantle wedges in subduction zones, based on the low P contents in arc volcanic rocks (e.g., Elliott et al., 1997; Togashi et al., 2000).

Arsenic was detected in many grains of antigorite and magnetite by electron microprobe analysis, although the concentrations of As are overall low (Table 2). The site and valence of As in silicate and oxide minerals are poorly known, but it was suggested that the small radius of As^{V} (0.6 Å) may allow it to reside in tetrahedral sites of silicate minerals by substituting for Si^{IV} (0.54 Å) (Esson et al., 1965; Smedley and Kinniburgh, 2002). This is supported by

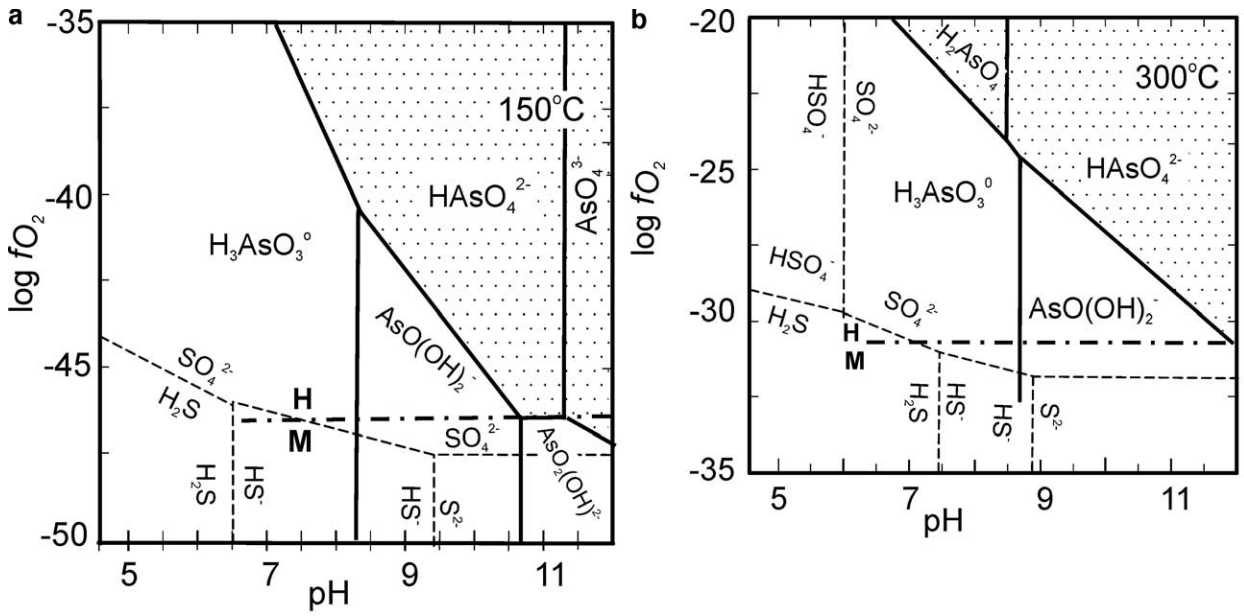

Fig. 7. Stability of dissolved As species at 150°C and 300°C at water vapor pressures. Dashed lines = boundaries between predominant dissolved sulfur species; thick dot-dashed lines = stability boundary between hematite (H) and magnetite (M); shaded areas = stable fields for oxidized As(V)-bearing species. Scorodite ($Fe^{III}As^{V}O_4 \cdot 2H_2O$) is not stable in ranges of pH and fO_2 shown here unless solutions contain unrealistically high Fe concentrations. Diagrams constructed using data of Shock et al. (1997) and Pokrovski et al. (1996) with aid of Helgeson-Kirkham-Flower model for aqueous species in FreeGs program, distributed by Geoscience Australia (Bastrakov et al., 2004).

relatively high Al_2O_3, up to 2.5 wt %, in antigorites with elevated concentrations of As, because the presence of Al(III) in Si^{IV}-O tetrahedra can compensate for the charge imbalance where Si(IV) is substituted by As(V). Furthermore, antigorite does not have a rigid crystallographic structure, which may facilitate a substantial substitution of ions with different valences, such as Si(IV) by As(V).

Arsenic may be sorbed on the surface of fine-grained serpentine minerals since sheet silicates have high sorption coefficients for As(V) (e.g., Smedley and Kinniburgh, 2002). Magnetite disseminated in serpentine is another possible mineral that may adsorb As(V), as As(V) is known to form relatively strong chemical bonds with metal oxide surfaces (e.g., Takahashi et al., 2004). Although reasonable size grains of magnetite do occur in antigorite, most grains of Fe-oxides in our samples are fine-grained with irregular shape, suggesting high surface areas. Adsorption of elements on mineral surfaces is well documented at low temperatures, but it may also be important at elevated temperatures. For example, Au- and As-bearing Fe-sulfides are known in many hydrothermal ore deposits, and the enrichment of As and Au in sulfides has been explained by their adsorption from aqueous fluids at temperatures ranging from 300° to 550°C, followed by their incorporation into sulfide crystal structures (e.g., Fleet and Mumin, 1997; Scaini et al., 1998; Simon et al., 1999). In our study, although it was not possible to obtain the concentrations of As on the surface, it is probable that As(V) was adsorbed on their surface and that it may be still present on their surface. Some of As may have led to subsequent incorporation into their crystal structures.

4.2. Source of Arsenic

The subduction zone where our serpentinite samples formed has a long history starting with the subduction of Tethyan oceanic crust followed by the subduction of the Indian continental margin. This long history of subduction, more than 100 m.y., may have contributed to the enrichment of As and other soluble elements in our samples. Furthermore, the margin of the Indian continent was overlain by shallow water sediments, of which protoliths are granitic rocks in the interior of the continent. Such sediments were most likely high in As because of their granitic source and depositional environments, since granitic rocks contain higher concentrations of As than mafic rocks. Furthermore, shallow-water sediments are commonly highly enriched in As compared to their sources in general (Onishi and Sandell, 1955; Togashi et al., 2000). These factors likely contributed to high As contents in the serpentinite samples.

There are two types of As in crustal rocks and sediments. The first type is As(III) or As(−1) in the structure of sulfides and organic compounds (Bose and Sharma, 2002; Smedley and Kinniburgh, 2002). This structurally bound As is minor in most crustal rocks except for sulfide-rich sediments (Smedley and Kinniburgh, 2002). The second type is As(V) adsorbed on organic matter, clays and Fe-Mn oxy-hyroxides. This type of As is more abundant and volumetrically important, especially in sediments. Among the adsorbents, Fe-oxides are the most important in crustal rocks because of their greater abundance in sediments and their strong binding affinity for As(V) (Smedley and Kinniburgh, 2002).

The first type of As, structurally bound in minerals, is re-

leased only when the host phases are destabilized. On the other hand, the second type of As, adsorbed As(V), is readily released from sediments to pore water during changes in chemical environments, such as pH, salinity, temperature and redox conditions (Smedley and Kinniburgh, 2002; Takahashi et al., 2004).

The high abundance of As(V) in our samples with elevated As concentrations (Fig. 5) suggests that the source of As was As(V), most likely released by desorption from sediments and slabs during the early stage of subduction. This is supported by low concentrations of As in metamorphosed rocks, as compiled for a variety of rocks by Onishi and Sandell (1955) and Togashi et al. (2000). The data suggest that As is released from rocks even during greenschist-facies metamorphism. This is in accord with the systematic analysis of As concentrations in the Catalina Schist, considered to represent subducted sediments, where As contents sharply decrease in higher grade epidote-bearing rocks (Bebout et al., 1999). Such data are consistent with As being released from subducted sediments and slabs at relatively low temperatures, $<$350°C, and thus shallow depths, $<$ 25 km.

The argument that As and other soluble elements were present in the samples before the subduction process is not supported because it would require that As(V) was present in the anhydrous mantle peridotites. This is highly unlikely given that high As contents have not been reported in anhydrous mantle peridotites. Furthermore, As in anhydrous mantle peridotites, if there is any, is likely to be As(III) because of the generally reduced conditions in the mantle.

It may be further argued that As was incorporated during the exhumation of serpentinites. This can be discounted because once hydrated, serpentinites do not incorporate much water and water-soluble elements. Furthermore, the exhumation of our serpentine samples was accompanied by minor dehydration, forming secondary olivine (Fo 96) and talc from antigorite (Guillot et al., 2001). Veinlets of chlorite, chrysotile, and minor calcite formed at a much later date, but they are easily identified and were excluded from analysis.

Sample CH 35A, from the base of the Nidar ophiolite, is quite different from the rest of samples, as it contains mostly As(III). This peridotite, likely hydrated during obduction of the Nidar arc, did not receive a continuous flux of water from an external, oxidized source. A low water/rock ratio during the serpentinization likely kept the serpentinite at a reduced state because release of Fe(II) from olivine commonly maintains a low fO_2 during hydration (Palandri and Reed, 2004).

4.3. Transfer of Arsenic from Slabs to Mantle Wedge

Arsenic is highly soluble in aqueous fluids as hydroxide complexes, such as $H_2As^{III}O_3^0$ and $HAs^vO_4^{2-}$, and its solubility increases at elevated temperatures (e.g., Pokrovski et al., 1996; Shock et al., 1997). Arsenic may be transported also in the vapor phases, as $As^{III}(OH)_3$ and $As^{V}O(OH)_3$, especially at high temperatures (Pokrovski et al., 2002). Another possible process for the transport of As(V) involves the release of As(V) from minerals in subducting slabs an sediments. As(V) in minerals likely stay as its oxidation state as far as the host minerals are stable. Disintegration of such minerals in subducted slabs and sediments would release As(V) into fluids to the overlying mantle wedges. We consider this as a minor component because As incorporated in minerals is minor in sediments and slabs.

Although As would be easily transported in subduction zones, an evaluation of the environment of As transport is not easy because the thermodynamic properties of aqueous As species, especially for As(V) species, are not well defined at elevated temperatures. This poses large uncertainties in the estimates of the stability fields of aqueous As species at elevated temperatures. However, the available data suggest that aqueous As(V) species are stable over a wide range of temperatures (Shock et al., 1997). They are stable at high pH and fO_2, and their stability fields overlap with those of sulfate (Figs. 7a,b).

Fluids that hydrate peridotites become alkaline as the hydration reaction proceeds (e.g., Normand et al., 2002), and alkaline solutions, with pH $>$11, are common in association with the hydration of ultramafic rocks (e.g., Barnes and O'Neil, 1969; Bruni et al., 2002; Kelley et al., 2005). This evidence suggests that As(V) released from sediments and slabs is likely stable in such highly alkaline conditions during the serpentinization of peridotites. The As concentration of the fluids during serpentinization increases as water is consumed by continuous hydration reactions, and the solutes are eventually fixed in the serpentinite minerals. Once As(V) is adsorbed onto or incorporated into mineral phases in serpentinites, it will likely retain its oxidation state.

The oxidized conditions during serpentinization of our samples may seem odd because highly reduced conditions are associated with the hydration of some peridotites (e.g., Sleep et al., 2004). Minerals indicative of reduced conditions are reported from serpentinites, such as native Fe and awaruite ($Ni_{2-3}Fe$), and graphite. Our samples lack such minerals, which is consistent with their oxidized condition.

What were the causes for the high oxidized state of our samples? First, our samples directly overlaid the subduction plane, thus they were continuously exposed to aqueous fluid from dehydrating slabs and sediments. Such a high flux of water likely maintained a high oxidation state during the hydration of peridotites. Second, gypsum in subducted evaporite beds likely acted as an oxidant of our serpentinite samples. There are abundant evaporate beds with gypsum and anhydrite on the northern margin of the Indian continent (e.g., Gaetani et al., 1986; Steck et al., 1993), and some of these evaporites were undoubtedly subducted beneath Eurasia based on the relics of evaporitic rocks in the Tso Morari eclogitic unit (Colchen et al., 1994).

Our proposed interpretation is consistent with low abundance of sulfides, $<$ 51 ppm S, and the limited range of $\delta^{34}S$ in our samples (Table 1). Sulfide minerals were not stable where our samples formed because of the oxidized conditions of serpentinization. The absence of sulfides in our samples contrast with sulfide-rich serpentinites formed under a low flux of water, which show a large range in $\delta^{34}S$ values due to a variable degree of sulfate reduction (e.g., Alt et al., 1998).

Our proposed interpretation, fluid transfer of oxidized As(V) from slabs to mantle wedges, is comparable to the transfer of U(VI) from slabs to mantle wedges. High U/Th ratios are noted in many arc magmas, attributed to the transfer of fluid-mobile U(VI) from subducting slabs to arc magmas via mantle wedges (e.g., Sigmarsson et al., 1990; Elliott et al., 1997; Hawkesworth

et al., 1997). Uranium in surface environments occurs as oxidized U(VI) species which are easily reduced to immobile U(IV), even during the diagenesis of sediments and in ground waters (e.g., Suzuki and Banfield, 1999). The release of U(VI) from slabs to mantle wedges also requires an oxidized state at the interface between slabs and overlying mantle wedges. Elevated U/Th ratios common in arc magmas suggest that oxidized conditions are not rare along subduction planes.

4.4. Transfer of Fluid-Soluble Elements to Arc Magmas

Partial melting that leads to the generation of arc magmas takes place in mantle wedges in response to an influx of water from subducting slabs and sediments (e.g., Tatsumi, 1986). However, the process by which water and soluble elements are transferred from slabs to the interior of the mantle wedge is in debate (e.g., Mibe et al., 1999; Hattori and Guillot, 2003). The most widely held view involves the rapid release of water from slabs during the eclogitization of slabs (e.g., Tatsumi, 1986; Peacock, 1993; Peacock and Wang, 1999). The water is suggested to form amphiboles in the overlying mantle wedge and their breakdown leads to partial melting.

Several workers have noted the problems associated with this model. First, the transformation of slabs to eclogites would occur at much shallower depths than expected (e.g., Fukao et al., 1983; Schmidt and Poli, 1998). Slabs are already eclogitized beneath the volcanic fronts. Second, water is continuously released from subducting slabs and overlying sediments in the fore arc region where the interior of the mantle wedge is hot enough for partial melting to occur (e.g., Schmidt and Poli, 1998), but the is no evidence here for partial melting. Furthermore, Sb is highly enriched in arc magmas (e.g., Noll et al., 1996), but it is a high-field strength element and should be retained in slabs during the eclogitization (Zack et al., 2002). Such enrichment can only be explained by its release from slabs at shallower depths before the eclogitization of slabs. A similar conclusion is reached from B isotope data of forearc serpentinites (Benton et al., 2001) and arc magmas in the Mariana arc (Straub and Layne, 2002). Boron is released during the early stage of subduction and is stored in the overlying mantle wedges.

We proposed a layer of serpentinites at the base of wedges as a sink for water and such highly fluid-mobile elements (Hattori and Guillot, 2003). This can explain the lack of volcanism in the forearc region because the serpentine layers would insulate the interior of wedges and keep it dry. Our proposed model is further supported by this study of the speciation of As, whereby As is released from slabs as As(V) early in subduction and is transferred to the overlying mantle wedge by fluids, to be incorporated in the serpentinite layer at its base.

When the serpentinite layer is transported downward by mantle flow, the As(V) is also transported with the serpentinites to hotter and deeper levels in the mantle. Thus, elements that may be released from the slab at low temperatures are transported with the serpentinites to deeper parts of the mantle. The stability of serpentine minerals is pressure-sensitive, and eventual dehydration of serpentine minerals causes a discharge of water and soluble elements at a depth of ~100 km (Hattori and Guillot, 2003). Arsenic and other soluble elements are not easily included in silicate minerals in the mantle and so are incorporated into the partial melt, although As may also be partially included in sulfides in the mantle wedge (Hattori et al., 2004).

In the mantle, As is reduced to As(III) in silicate melt or As (−1) in sulfides. The presence of As(III) in melt is suggested based on the presence of As(III) in high-temperature volcanic gases and magmatic hydrothermal fluids (Onishi and Sandell, 1955; Smedley and Kinniburgh, 2002). This implies the reduction of As(V) to As(III) or As(−1) in the interior of the mantle wedge. Although As is minor in concentration compared to S and Fe(III), reduction of As(V) will contribute to the oxidation of mantle wedges.

5. SUMMARY

Strong absorption peaks at around 11.87 keV in XANES spectra suggest that As in serpentinite samples is mostly As(V), bonded with O. Arsenic present in sulfide minerals and arsenides is minor, despite high concentrations of As in a few sulfide grains and the finding of one grain of Ni arsenide. The abundance of As(V) is further confirmed by structural parameters obtained from EXAFS spectra of one sample, compared to reference materials. The fraction of As(V) to the total As increases in samples with higher concentrations of As, indicating that As was introduced to the mantle peridotites as the oxidized species As(V). This As was most likely derived from As(V) released from sediments and slabs by desorption at a relatively shallow depth in a subduction zone along with other fluid-soluble elements. The subduction of evaporites and a continuous flux of water from slabs to the overlying mantle wedge likely kept the serpentinites at the base of the mantle wedge in an oxidized state. Once As(V) was incorporated into serpentinite minerals, it likely retained its valence in the mantle and was transported together with the host to deep levels, ~100 km, of the mantle before final exhumation with the Tso Morari eclogitic unit.

Acknowledgments—We thank Ron Hartree for XRF analysis, Wendy Abdi for the determination of S concentrations and isotope compositions, George Mrazek for preparation of thin sections, and Monika Wilk-Alemany for assisting in the other laboratory analysis. The XAFS experiments were made possible with the approval of KEK-PF (proposal 2004G119) and JASRI-SPring-8 (proposal 2004A0617-NXa-np). This study was supported by grants from NSERC in Canada, the Ministry of Education, Science, Sports and Culture of Japan, and CNRS France. The manuscript was completed during a Japan Society for the Promotion of Science Invitation Fellowship to KHH at JAMSTEC. We thank J. C. Alt, J. Hedenquist, J. G. Ryan, and an anonymous journal reviewer for their comments.

Associate editor: J. C. Alt

REFERENCES

Alt J. C. and Shanks W. C. III. (1998) Sulfur in serpentinized oceanic peridotites: Serpentinization processes and microbial sulphate reduction. *J. Geophys. Res.* **103,** 9917–9929.

Ando A., Kamioka H., Terashima S. and Itoh S. (1989) 1988 values for GSJ rock reference samples, "Igneous rock series". *Geochim. J.* **23,** 143–148.

Ankudinov A. L. and Rehr J. J. (1997) Relativistic calculations of spin-dependent x-ray absorption spectra. *Phys. Rev. B* **56,** 1712–1716.

Barnes I. and O'Neil J. R. (1969) The relationship between fluids in some fresh Alpine-type ultramafics and possible modern serpenti-

nization, western United States. *Geol. Soc. Am. Bull.* **80,** 1947–1960.

Bastrakov E., Shvarov Y., Girvan S., Vleverley J., and Wyborn L. (2004) FreeGs: Web-based thermodynamic data base for modelling of geochemical processes. In *Dynamic Earth: Past, Present and Future* (eds. J. McPhie and P. McGoldrick), p. 52. 17th Australian Geological Convention Hobart, Vol. 73.

Bebout G. E., Ryan J. G., Leeman W. P., and Bebout A. E. (1999) Fractionation of trace elements by subduction-zone metamorphism-effect of convergent-margin thermal evolution. *Earth Planet. Sci. Lett.* **171,** 63–81.

Benton L. D., Ryan J. G., and Tera F. (2001) Boron isotope systematics of slab fluids as inferred from a serpentine seamount, Mariana forearc. *Earth Planet. Sci. Lett.* **187,** 273–282.

Bernard A., Knittel U., Weber B., Weis D., Albrecht A., Hattori K., Klein J., and Oles D. (1996) Petrology and geochemistry of the 1991 eruption products of Mount Pinatubo. In *Fire and mud: eruptions and lahars of Mount Pinatubo, Philippines* (eds. C. G. Newhall and R. S. Punongbayan) PHIVOLCS, Quezon City, Philippines and University of Washington Press, Seattle. pp 767–797.

Bose P. and Sharma A. (2002) Role of iron in controlling speciation and mobilization of arsenic in subsurface environment. *Water Resources* **36,** 4916–4926.

Brown G. E. Jr., Calas G., Waychunas G. A., and Petiau J. (1988) X-ray absorption spectroscopy and its applications in mineralogy and geochemistry. *Rev. Mineral.* **18,** 431–512.

Bruni J., Marco C., Giovanni C., Roberto C., Francesco C., Antonio L., Luigi M., Guilio O., and Marino V. Z. (2002) Irreversible water-rock mass transfer accompanying the generation of the neutral, Mg-HCO_3 and high pH, Ca-OH spring waters of the Genova Province, Italy. *Appl. Geochem.* **17,** 455–474.

Colchen M., Mascle G., and Delaygue G. (1994) Lithostratigraphy and age of the formation of the Tso Morari dome. 9th Himalayan-Karakoram-Tibet Workshop, Kathmandu. *J. Geol. Soc. Nepal* **10,** 23–24.

Elliott T., Plank T., Zindler A., White W., and Bourdon B. (1997) Element transport from slab to volcanic front at the Mariana arc. *J. Geophys. Res.* **102,** 14991–15019.

Emmerling F. and Roehr C. (2003) Die neuen Oxoarsenate(III) $AAsO_2$ (A= Na, K, Rb) und $Cs_3As_5O_9$. Darstellung, Kristallstrukturen und Raman-Spektren. *Z. Naturforsch. B* **58,** 620–626.

Esson J., Stevens R. H., and Vincent E. A. (1965) Aspects of the geochemistry of arsenic and antimony, exemplified by the Skaergaard intrusion. *Min. Mag.* **35,** 88–107.

Fenter P. A., Rivers M. L., Sturchio N. C., and Sutton S. R. (2002) Applications of synchrotron radiation in low-temperature geochemistry and environmental science. Reviews in Mineralogy and Geochemistry 49. Mineralogical Society, Washington, D.C.

Fleet M. E. and Mumin A. H. (1997) Gold-bearing arsenian pyrite, marcasite and arsenopyrite from Carlin trend gold deposits and laboratory synthesis. *Am. Mineral.* **82** 182–193.

Fukao Y., Hori S., and Ukawa M. (1983) A seismological constraint on the depth of basalt-eclogite transition in a subducting oceanic crust. *Nature* **303,** 413–415.

Gaetani M., Casnedi R., Fois E., Garzanti E., Jadoul F., Nicora A., and Tintori A. (1986) Stratigraphy of the Tethys Himalaya in Zanskar, Ladakh. *Riv. Ital. Paleont. Stratigr.* 443–478.

Gill J. B. (1981) *Orogenic Andesites and Plate Tectonics.* Springer-Verlag, New York.

Guillot S., Hattori K., de Sigoyer J., Nägler T., and Auzende A. L. (2001) Evidence of hydration of the mantle wedge and its role in the exhumation of eclogites. *Earth Planet. Sci. Lett.* **193,** 115–127.

Guillot S., Hattori K. H., and de Sigoyer J. (2000) Mantle wedge serpentinization and exhumation of eclogites: Insights from eastern Ladakh, NW Himalaya. *Geology* **28,** 199–202.

Hageman P. L., Brown Z. A., and Welsch E. (2002) Arsenic and selenium by flow injection or continuous flow-hydride generation-atomic absorption spectrometry. Open-File. Rreport 02-223, L1–L7. U.S. Geological Survey.

Hattori K. H. and Guillot S. (2003) Volcanic fronts as a consequence of serpentinite dehydration in the mantle wedge. *Geology* **31,** 525–528.

Hattori K. H., Cabri L. J., Johanson B., and Zientek M. L. (2004) Origin of placer laurite from Borneo: Se and As contents and S isotopic compositions. *Min. Mag.* **68,** 353–368.

Hawkesworth C. J., Turner S. P., McDermott F., Peate D. W., and van Calesteren P. (1997) U-Th isotopes in arc magmas: Implications for element transfer from the subducted crust. *Science* **276,** 551–555.

Henao J. A., Diaz de Delgado G., Delgado J. M., Castrillo F. J., and Odreman O. (1994) Single-crystal structure refinement of enargite (Cu_3AsS_4). *Material. Res. Bull.* **29,** 1121–1127.

Hugging F. E., Shah N., Zhao J., Lu F., and Huffman G. P. (1993) Nondestructive determination of trace element speciation in coal and coal ash by XAFS spectroscopy. *Energy Fuels* **7,** 482–489.

Kelley D. S., Karson J. A., Fruh-Green G. L., et al. (2005) A serpentinite-hosted ecosystem: The Lost City hydrothermal field. *Science* **307,** 1428–1434.

Leeman W. P. (1996) Boron and other fluid-mobile elements in volcanic arc lavas: Implications for subduction processes. *Geophys. Union Monogr.* **96,** 269–276.

Locock A. J., Burns P. C., and Flynn T. M. (2005) The role of water in the structures of synthetic hallimodite, $Pb_2[(UO_2)(AsO_4)_2](H_2O)_n$ and synthetic parsonsite, $Pb_2[(UO_2)(PO_4)_2](H_2O)_n$, $0 \leq n \leq 0.5$. *Am. Mineral.* **90,** 240–246.

Mahéo G., Bertrand H., Guillot S., Villa I. M., Keller F., and Capiez P. (2004) The South Ladakh ophiolite (NW Himalaya, India): An intra-oceanic tholeiitic arc origin with implication for the closure of the Neo-Tethys. *Chem. Geol.* **203,** 273–303.

McDonough W. and Sun S. S. (1995) The composition of the Earth. *Chem. Geol.* **120,** 223–253.

Mibe K., Fujii T., and Yasuda A. (1999) Control of the location of the volcanic front in island arcs by aqueous fluid connectivity in the mantle wedge. *Nature* **401,** 259–262.

Mihajlović T. and Effenberger H. (2004) The first proof of protonated anion tetrahedral in the tsumcorite-type compounds. *Min. Mag.* **68,** 757–767.

Morimoto N. and Clark L. A. (1961) Arsenopyrite crystal-chemical relations. *Am. Mineral.* **46,** 1448–1469.

Noll P. D. Jr., Newsom H. E., Leeman W. P., and Ryan J. G. (1996) The role of hydrothermal fluids in the production of subduction zone magmas: Evidence from siderophile and chalcophile trace elements and boron. *Geochim. Cosmochim. Acta* **60,** 587–611.

Normand C., Williamds-Jones A. E., Martin R. F., and Hojatollah V. (2002) Hydrothermal alteration of olivine in a flow-through autoclave; nucleation and growth of serpentinie phases. *Am. Mineral.* **87,** 1699–1709.

O'Day P. A., Rehr J. J., Zabinsky S. I., and Brown G. E. (1994) Extended X-ray absorption fine structure (EXAFS) analysis of disorder and multiple scattering in complex crystalline solids. *J. Am. Chem. Soc.* **116,** 2938–2949.

O'Day P. A., Rivera N. Jr., Root R., and Carroll S. A. (2004) X-ray absorption spectroscopic study of Fe reference compounds for the analysis of natural sediments. *Am. Mineral.* **89,** 572–585.

Onishi H. and Sandell E. B. (1955) Geochemistry of arsenic. *Geochim. Cosmochim. Acta* **7,** 1–33.

Palandri J. L. and Reed M. H. (2004) Geochemical models of metasomatism in ultramafic systems: Serpentinization, rodingtization and sea floor carbonate chimney precipitation. *Geochim. Cosmochim. Acta* **68,** 1115–1133.

Peacock S. M. (1993) Metamorphism, dehydration, an dimportance of the blueschist-eclogite transition in subducting oceanic crust. *Geo. Soc. Am. Bull.* **105,** 684–694.

Peacock S. M. and Wang K. (1999) Seismic consequences of warm versus cool subduction metamorphism: Examples from southwest and northeast Japan. *Science* **286,** 937–939.

Pertlik F. (1978) Structure refinement of cubic As_2O_3 (arsenolite) with single crystal data. *Czech. J. Phys.*, **28,** 170–176.

Pertlik F. (1994) Kristallstrukturbestimmung der monoklinen Hochtemperaturmodifikation von AsS (α-AsS). *Österreichische Akad. Wissenschaften (Austrian Acad. Sci.) Math.-Natur. Sitzungsberichte* **131,** 3–5.

Pokrovski G., Gout R., Shott J., Zotov A., and Harrichoury J.-C. (1996) Thermodynamic properties and stoichiometry of As(III) hydroxide complexes at hydrothermal conditions. *Geochim. Cosmochim. Acta* **60,** 737–749.

Pokrovski G. S., Zakirov I. V., Roux J., Testemale D., Hazemann J-L., Bychkov A. Y., and Golikova G. V. (2002) Experimental study of arsenic speciation in vapour phase to 500°C: Implications for As transport and fractionation in low-density crustal fluids and volcanic gases. *Geochim. Cosmochim. Acta* **66,** 3453–3480.

Ravel B. (2001) ATOMS: Crystallography for the X-ray absorption spectroscopy. *J. Synchrotron Rad.* **8,** 314–316.

Ryan J. G., Morris J., Tera F., Leeman W. P., and Tsvdetkov A. (1995) Cross-arc geochemical variations in the Kurile arc as a function of slab depth. *Science* **270** 625–627.

Sasaki A., Arikawa Y., and Folinsbee R. E. (1979) Kiba reagent method of sulphur extraction applied to isotopic work. *Bull. Geol. Surv. Jpn.* **30,** 241–245.

Savage K. S., Tingle T. N., O'Day P. A., Waychunas G. A., and Bird D. K. (2000) Arsenic speciation in pyrite and secondary weathering phases, Mother Lode Gold district, Tuolumne County, California. *Appl. Geochem.* **15,** 1219–1244.

Scaini M. J., Bancroft G. M., and Knipe S. W. (1998) Reactions of aqueous Au^{1+} sulphide species with pyrite as a function of pH and temperature. *Am. Mineral.* **83,** 316–322.

Schmidt M. W. and Poli S. (1998) Experimentally based water budgets for dehydrating slabs and consequences for arc magma generation. *Earth Planet. Sci. Lett.* **163,** 361–379.

Shock E. L., Sassani D. C., Willis M. and Sverjensky D.A. (1997) Inorganic species in geologic fluids: Correlations among standard molal thermodynamic properties of aqueous ions and hydroxide complexes. *Geochim Cosmochim. Acta*, **61**, 907–950.

Sigmarsson O., Condomines M., Morris J. D., and Harmon R. S. (1990) Uranium and ^{10}Be enrichments by fluids in Andean arc magmas. *Nature* **346,** 163–165.

Simon G., Huang H., Penner-Hahn J. E., Kesler S. E., and Kao L. S. (1999) Oxidation state of gold and arsenic in gold-bearing arsenian pyrite. *Am. Mineral.* **84,** 1071–1079.

Sleep N. H., Meibom A., Fridriksson, Th., Coleman R. G., and Bird D. K. (2004) H_2-rich fluids from serpentinization: Geochemical and biotic implications. *Proc. Natl. Acad. Sci. U S A* **101,** 12818–12823.

Smedley P. L. and Kinniburgh D. G. (2002) A review of the source, behaviour and distribution of arsenic in natural waters. *Appl. Geochem.* **17,** 517–568.

Steck A., Spring L., Vannay J.-C., Masson H., Bucher H., Stutz E., Marchant R., and Tièche J.-C. (1993) Geological transect across the Northwestern Himalaya in eastern Ladakh and Lahul: A model for the continental collision of India and Asia. *Ecol. Geol. Helvetiae* **86,** 219–263.

Straub S. M. and Layne G. D. (2002) The systematics of boron isotopes in Izu arc front volcanic rocks. *Earth Planet. Sci. Lett.* **198,** 25–39.

Suzuki Y. and Banfield J. F. (1999) Geomicrobiology of uranium. *Rev. Mineral. Geochem.* **38,** 393–432.

Takahashi Y., Ohtaku N., Mitsunobu S., Yuita K., and Nomura M. (2003) Determination of the As(III)/As(V) ratio in soil by X-ray absorption near-edge structure (XANES) and its application to the arsenic distribution between soil and water. *Anal. Sci.* **19,** 891–896.

Takahashi Y., Minamikawa R., Hattori K. H., Kurishima K., Nihou N., and Yuita K. (2004) Arsenic behaviour in paddy fields during the cycle of flooded and non-flooded periods. *Environ. Sci. Technol.* **38,** 1038–1044.

Tatsumi Y. (1986) Formation of volcanic front in subduction zones. *Geophys. Res. Lett.* **13,** 717–720.

Togashi S., Imai N., Okuyama-Kusunose Y., Tanaka T., Okai T., Koma T., and Murata Y. (2000) Young upper crustal chemical composition of the orogenic Japan arc. *Goechem. Geophys. Geosystems* **1,** 2000GC000083.

Volynets O. N. (1994) Geochemical types, petrology, and genesis of late Cenozoic volcanic rocks from the Kuril-Kamchatka island-arc system. *Intern. Geol. Review* **36**, 373–405.

Zachariáš J., Fŕyda J., Paterová B., and Mihaljevič M. (2004) Arsenopyrite and As-bearing pyrite from the Roudňy deposit, Bohemian Massif. *Min. Mag.* **68,** 31–46.

Zack T., Kronz A., Foley S. F., and Rivers T. (2002) Trace element abundances in rutiles from eclogites and associated garnet mica schists. *Chem. Geol.* **184,** 97–122.

Zabinsky S. I., Rehr J. J., Ankudinov A., Albers R. C., and Eller M. J. (1995) Multiple Scattering Calculations of X-ray Absorption Spectra. *Phys. Rev. B* **52,** 2995–3009.